Type 1 ryanodine receptor knock-in mutation causing central core disease of skeletal muscle also displays a neuronal phenotype

Valerie De Crescenzo[a,1], Kevin E. Fogarty[b], Jason J. Lefkowitz[a], Karl D. Bellve[b], Elena Zvaritch[c], David H. MacLennan[c,1], and John V. Walsh, Jr.[a]

[a]Department of Microbiology and Physiological Systems, University of Massachusetts Medical School, Worcester, MA 01655; [b]Biomedical Imaging Group, University of Massachusetts Medical School, Worcester, MA 01605; and [c]Banting and Best Department of Medical Research, Charles H. Best Institute, University of Toronto, Toronto, ON, Canada M5G 1L6

Contributed by David H. MacLennan, September 19, 2011 (sent for review July 27, 2011)

The type 1 ryanodine receptor (RyR1) is expressed widely in the brain, with high levels in the cerebellum, hippocampus, and hypothalamus. We have shown that L-type Ca^{2+} channels in terminals of hypothalamic magnocellular neurons are coupled to RyRs, as they are in skeletal muscle, allowing voltage-induced Ca^{2+} release (VICaR) from internal Ca^{2+} stores without Ca^{2+} influx. Here we demonstrate that RyR1 plays a role in VICaR in nerve terminals. Furthermore, in heterozygotes from the *Ryr1*$^{I4895T/WT}$ (IT/+) mouse line, carrying a knock-in mutation corresponding to one that causes a severe form of human central core disease, VICaR is absent, demonstrating that type 1 RyR mediates VICaR and that these mice have a neuronal phenotype. The absence of VICaR was shown in two ways: first, depolarization in the absence of Ca^{2+} influx elicited Ca^{2+}syntillas (*scintilla*, spark, in a nerve terminal, a SYNaptic structure) in WT, but not in mutant terminals; second, in the presence of extracellular Ca^{2+}, IT/+ terminals showed a twofold decrease in global Ca^{2+} transients, with no change in plasmalemmal Ca^{2+} current. From these studies we draw two conclusions: (*i*) RyR1 plays a role in VICaR in hypothalamic nerve terminals; and (*ii*) a neuronal alteration accompanies the myopathy in IT/+ mice, and, possibly in humans carrying the corresponding *RyR1* mutation.

microdomain | exocytosis | oxytocin | vasopressin

In recent years evidence has accumulated for a role for Ca^{2+} stores in nerve terminals (1, 2). In isolated magnocellular terminals, we found spontaneous, focal, ryanodine-sensitive, cytosolic Ca^{2+} transients (Ca^{2+} syntillas). Quite unexpectedly, we also found that depolarization of the plasma membrane in the absence of external Ca^{2+} and, therefore, in the absence of Ca^{2+} influx, increased syntilla frequency and global [Ca^{2+}] (3). We designated this process, which had only been observed previously in skeletal muscle, as voltage-induced Ca^{2+} release (VICaR). At about the same time, evidence for VICaR was also found in dorsal column axons (4) and, more recently, in hippocampal pyramidal neurons (5). In addition we have demonstrated that VICaR in nerve terminals is mediated by ryanodine receptors (RyRs) and dihydropyridine receptors (DHPRs) as in skeletal muscle (6).

RyRs are large (2.2 MDa) homotetramers that reside in sarcoplasmic or endoplasmic reticulum membranes and function as Ca^{2+} release channels, conducting Ca^{2+} into the cytosol. All three RyR isoforms are present in the mammalian brain (7). Although Ca^{2+}-induced Ca^{2+} release (CICR) through RyR2 has been implicated in the amplification of Ca^{2+} transients in neurons, no role has yet been assigned to RyR1. Previously, we provided immunocytochemical evidence that in hypothalamic magnocellular nerve terminals RyR1 is located close to the plasma membrane, placing it in position to mediate VICaR, but so far there has been no functional evidence for a role of RyR1 in the terminals. In contrast to its uncertain role in the nervous system, RyR1 is known to play a key role in excitation-contraction (EC) coupling in skeletal muscle (8).

A growing number of skeletal muscle disorders have been associated with mutations in *RyR1*, the most frequent being malignant hyperthermia (MH) and core myopathies, such as central core disease (CCD) and multiminicore disease. By now, more than 300 disease-causative mutations have been identified in *RyR1* (9). *RyR1* mutations causing MH and CCD occur throughout the molecule, but there are three hotspots in which the frequency of mutations is increased (9). Some mutations in the third hotspot region, near the C terminus, perturb the structure of the Ca^{2+} pore and thus interfere directly with the intrinsic function of Ca^{2+} release. These mutations have been associated predominantly with core myopathies. One of these is the human *Ryr*^{I4898T} mutation, which is among the most frequent of those *RyR1* mutations that are associated with CCD and other core myopathies (10–12). The mutation is located in the selectivity filter of the Ca^{2+} pore (13) and disrupts Ca^{2+} permeation without affecting the overall structural and supramolecular organization of RyR1 (14–16).

We generated a knock-in mouse line, *Ryr1*$^{I4895T/WT}$ (herein referred to as IT/+), carrying the murine analog of the human I4898T mutation (16). In the homozygous state, this mutation is neonatally lethal because the mice have very poorly developed skeletal muscle, including that forming the diaphragm, and are unable to breathe (16). In the heterozygous state, depending on the background, the mouse mutation causes a progressive core myopathy with cores and rods, which significantly impairs mobility by about 1 y of age (14, 17, 18).

Congenital core myopathies are a group of neuromuscular disorders of highly variable pathology that typically present in infancy with skeletal muscle weakness, hypotonia, and delayed motor development (19). The existence of a neural component in the etiology of core myopathies has long been debated (20–22). The idea is based on the striking similarity between the core lesions observed in the skeletal muscle of patients with core myopathies and the targetoid lesions reported in denervated muscle (20–23) and after tenotomy (17). An abnormality in motor neuron function was thus proposed, but never proved experimentally. Moreover, the involvement of distinct components of the central nervous system in the etiology of core myopathies has also never been addressed. Because investigators have long debated the possibility that congenital myopathies have a neural component, we reasoned that IT/+ mice might provide a useful model for the investigation of a potential neural defect accompanying the manifestations of core myopathies. Here we demonstrate that IT/+ mice do, indeed, have a neuronal phenotype. Moreover, the genetic approach has

Author contributions: V.D.C., K.E.F., and J.V.W. designed research; V.D.C. and J.J.L. performed research; K.E.F., K.D.B., E.Z., and D.H.M. contributed new reagents/analytic tools; V.D.C., K.E.F., J.J.L., and J.V.W. analyzed data; and V.D.C., E.Z., D.H.M., and J.V.W. wrote the paper.

The authors declare no conflict of interest.

[1]To whom correspondence may be addressed. E-mail: valerie.decrescenzo@umassmed.edu or david.maclennan@utoronto.ca.

provided direct functional evidence that RyR1 mediates VICaR in nerve terminals.

Results

Ca^{2+} Syntilla Frequency Is Increased at −80 mV in IT/+ Compared with WT. Our first experiments were designed to examine whether Ca^{2+} syntillas were present in IT/+ hypothalamic magnocellular nerve terminals under conditions closely approximating the physiological resting state (i.e., in the presence of 2.2 mM extracellular Ca^{2+}) with the plasmalemmal potential held at −80 mV (Fig. 1*A*). Under these conditions, the nerve terminals display spontaneous Ca^{2+} syntillas and, surprisingly, frequency was increased more than threefold in the IT/+ mutant, from $0.23 \pm 0.06\ s^{-1}$ ($n = 22$) in the WT to $0.87 \pm 0.18\ s^{-1}$ ($n = 21$) in IT/+ nerve terminals ($P = 0.001$) (Fig. 1 *A* and *B1* and Table 1). The signal mass for WT was $44.20 \pm 10.28 \times 10^{-20}$ moles of Ca^{2+} ($N = 6$) and for the IT/+ mutant was $73.39 \pm 8.07 \times 10^{-20}$ moles of Ca^{2+} ($N = 43$), $P = 0.193$ (Fig. 1*B2* and Table 1). It is worth noting that the increase in syntilla frequency did not raise the resting cytosolic [Ca^{2+}] (31.77 ± 8.20 nM in IT/+ terminals vs. 51.32 ± 12.90 nM in WT, $P = 0.380$). Thus, at the level of spontaneous activity, the IT/+ mutant exhibits a neuronal phenotype at the level of cellular physiology.

Voltage-Induced Ca^{2+} Release, Present in the WT, Is Blocked in IT/+. Next we examined the effect of the mutation on VICaR. To observe VICaR, which demands depolarization of the terminal, we used a solution without extracellular [Ca^{2+}]. That process allowed us to avoid possible interference because of Ca^{2+} influx and to ensure that there is no CICR that is evoked by Ca^{2+} influx. Moreover, only in this Ca^{2+}-free condition can an increase in frequency of syntillas be seen, because syntillas are not obscured by a global increase in [Ca^{2+}]. Depolarization of nerve terminals from −80 to 0 mV induced an increase in syntilla frequency from $0.98 \pm 0.24\ s^{-1}$ ($n = 14$) at −80 mV to $2.75 \pm 0.56\ s^{-1}$ at 0 mV ($n = 7$), $P = 0.003$ (Fig. 2 *A* and *B1* and Table1), demonstrating VICaR in the terminals of the WT sv129 mouse strain. The increase in frequency was similar to our earlier findings in Swiss Webster mice (6). However, with the nerve terminals of sv129 IT/+ litter mates, syntilla frequency was not changed significantly upon depolarization ($1.78 \pm 0.25\ s^{-1}$ ($n = 8$) at −80 mV and $1.00 \pm 0.60\ s^{-1}$ ($n = 7$) at 0 mV). Because the signal mass of syntillas recorded in WT and IT/+ terminals at 0 mV was similar [$79.3 \pm 6.6 \times 10^{-20}$ moles of Ca^{2+} ($N = 68$) in the WT vs. $98.0 \pm 16.1 \times 10^{-20}$ moles of Ca^{2+} ($N = 28$) in IT/+] (Fig. 1*B2* and Table 1), the absence of VICaR in the mutant could not be because of undetected syntillas. We conclude that the IT/+ mutation induces a loss of VICaR, as measured by syntilla frequency.

We also observed an unusually large signal mass of the syntillas in the WT sv129 at −80 mV [$220.6 \pm 30.1 \times 10^{-20}$ moles of Ca^{2+} ($N = 40$)] (Fig. 2*B2* and Table 1) in the Ca^{2+}-free condition, which is not seen in Swiss Webster (3) and may represent a heightened susceptibility of the sv129 nerve terminals to the nonphysiological conditions of the Ca^{2+}-free environment.

Global Ca^{2+} Transient Upon Depolarization Is Reduced Twofold in IT/+ Compared with WT. We next examined the effect of the absence of VICaR in IT/+ nerve terminals in the presence of 2.2 mM external Ca^{2+} during depolarization, which raised global [Ca^{2+}]. We compared IT/+ and WT take away and nerve terminals upon depolarization to 0 mV using ratiometric fura-2 measurements (Fig. 3*A*). The increase in fura-2 ratio in IT/+ was two-thirds of the value in WT (1.29 in IT/+ vs. 1.92 in WT, $P = 0.009$). At this potential (0 mV), the magnitude of the plasmalemmal peak Ca^{2+} current (Fig. 3*B*) was not significantly different in WT and IT/+ terminals −34.27± 7.18 pA ($n = 10$) in IT/+ vs. −44.95 ± 10.85 pA ($n = 6$) in WT ($P = 0.375$). Thus, the difference in the global transients does not appear to be caused by changes in Ca^{2+} influx but rather indicates a defect in Ca^{2+} release from intracellular stores. Because these experiments were carried out under the same conditions in which the mutant was studied in skeletal muscle, a comparison is possible, and the results in the nerve terminal are comparable to those in skeletal fibers (15).

IT/+ and WT Respond Differently to Physiological Stimulation Protocols. We then asked whether a mutant *RyR1* phenotype was apparent in the nerve terminals during protocols used to mimic physiological activation. The nerve terminals were stimulated either by a prolonged depolarization to mimic the depolarization caused by K^+ accumulation outside the nerve terminals (Fig. 4*A*) (24) or a train of short depolarizations to mimic a burst of action potentials (NS80 in Fig. 4*C*) (24, 25). Global Ca^{2+} transients were measured with fluo-3, which is sufficiently rapid to give an indication of the rate of rise of the transients (26). With the long depolarization paradigm (Fig. 4*A*), the Ca^{2+} transient in IT/+ [red trace, 1.46 ± 0.11 ($n = 9$)] was significantly smaller than that in WT [blue trace, 2.51 ± 0.13 ($n = 12$)], as expected from the fura-2 data in Fig. 3*A* that were recorded under the same conditions (i.e., with 2.2 mM external Ca^{2+} and prolonged depolarization).

In the presence of Cd^{2+} to block Ca^{2+} current, the Ca^{2+} transient in WT decreased from 2.51 ± 0.13 ($n = 12$) to 1.52 ± 0.17 ($n = 12$), $P = 0.00013$; the magnitude of the remaining transient can be taken as the component elicited by VICaR. Thus, consistent with our earlier findings, long depolarizations were able to induce VICaR in WT. However, in IT/+ terminals, in the presence of Cd^{2+}, we observed a very slow and small increase in global Ca^{2+} [1.21 ± 0.05 ($n = 9$), compared with 1.52 ± 0.17 ($n = 12$, $P = 0.05$) in the absence of Cd^{2+}], indicating that in IT/+ terminals VICaR is quite small. In each case, the increase in global [Ca^{2+}] made it difficult to monitor syntillas due to the increase in background fluorescence.

Loy et al. (15) showed that single skeletal muscle fibers from IT/+ mice exhibited a significant reduction in both the magnitude and maximum rate of RyR1-mediated Ca^{2+} release during EC coupling. To determine whether a similar slowing exists in nerve terminals, we compared the kinetics of Ca^{2+} release in WT and IT/+ terminals during the long depolarization that was able

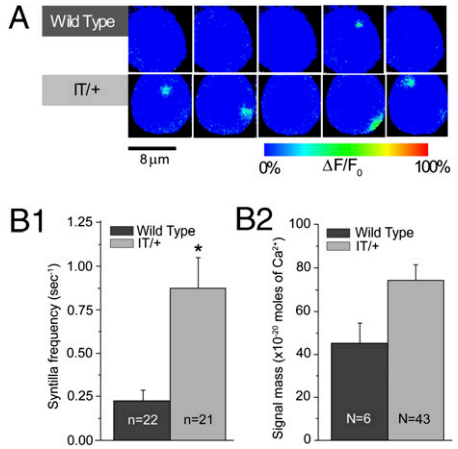

Fig. 1. Spontaneous Ca^{2+} syntillas are increased in IT/+nerve terminals. Terminals are voltage-clamped at −80 mV in the presence of 2.2 mM extracellular Ca^{2+}, with fluo-3 in the patch pipette. (*A*) Representative records of syntillas in WT (*Upper*) and IT/+ (*Lower*) terminals. (*B1*) Ca^{2+} syntilla frequency in IT/+ terminals is increased to $0.87 \pm 0.18\ s^{-1}$ ($n = 21$) compared with $0.23 \pm 0.06\ s^{-1}$ ($n = 22$) in WT ($P = 0.001$); (*B2*) the signal mass is not significantly different for WT and IT/+. Here and in subsequent figures, *N* is the number of syntillas and *n*, the number of experiments. *$P < 0.05$.

Table 1. Data summary

		Frequency (s^{-1})		Signal mass × 10^{-20} moles of Ca^{2+}	
Solution	Voltage	WT	IT/+	WT	IT/+
2.2 mM Ca^{2+}	−80 mV	0.23 ± 0.06	0.87 ± 0.18	44.20 ± 10.28	73.39 ± 8.07
	0 mV	Global increase	Global increase	Global increase	Global increase
Ca^{2+}-free	−80 mV	0.98 ± 0.24	1.78 ± 0.25	220.6 ± 30.1	124.3 ± 13.9
	0 mV	2.75 ± 0.56	1.00 ± 0.60	79.3 ± 6.6	98.0 ± 16.1

Summarization of the syntilla frequency and signal mass data collected for Figs. 1 and 2.

to elicit VICaR in WT (Fig. 4*B*). We have shown previously that fluo-3 was fast enough to study the time course of sparks in smooth muscle (27) and syntillas in nerve terminals (3). The binding kinetics of fluo-3 (26) are also sufficient to reveal differences in the Ca^{2+} transient time course, which appears slower in this system than in skeletal muscle. The maximum rate of Ca^{2+} release was approximated from the peak of the first derivative of the fluo-3 fluorescence (d[Δ*F*/*F*]/dt) (Fig. 4*B*). The maximum rate of Ca^{2+} release is significantly reduced in IT/+ nerve terminals (0.8 ± 0.3) compared with WT (2.7 ± 0.3, $P = 0.0014$). Moreover, in the presence of Cd^{2+}, where only VICaR is recorded, no increase in Ca^{2+} release was evident in the IT/+ terminals.

With the NS80 protocol (Fig. 4*C*), we did not observe a difference in the F/F_0 increase between WT and IT/+. Moreover, in the presence of Cd^{2+}, there was no indication of VICaR in WT or IT/+ by monitoring global Ca^{2+}. However, because there was no global increase in Ca^{2+} when Cd^{2+} was present, we were able to monitor syntillas, which was not possible with the long depolarization protocol (Fig. 4*A*). In the presence of Cd^{2+}, we observed a significant increase in syntilla frequency in WT terminals (from 0.36 ± 0.08 s^{-1} at −80 mV to 0.85 ± 0.13 s^{-1} under NS80, $P = 0.019$). Hence, it appears that the prolonged depolarization protocol is more effective than the NS80 protocol at eliciting VICaR. With the prolonged depolarization protocol, VICaR causes an increase in global [Ca^{2+}], whereas with the NS80 protocol the increase in syntilla frequency does not coalesce into an increase in global [Ca^{2+}]. In the IT/+ terminals in the presence of Cd^{2+}, VICaR was not demonstrable (syntilla frequencies were 0.48 ± 0.11 at −80 mV and 0.69 ± 0.16 under NS80 in IT/+).

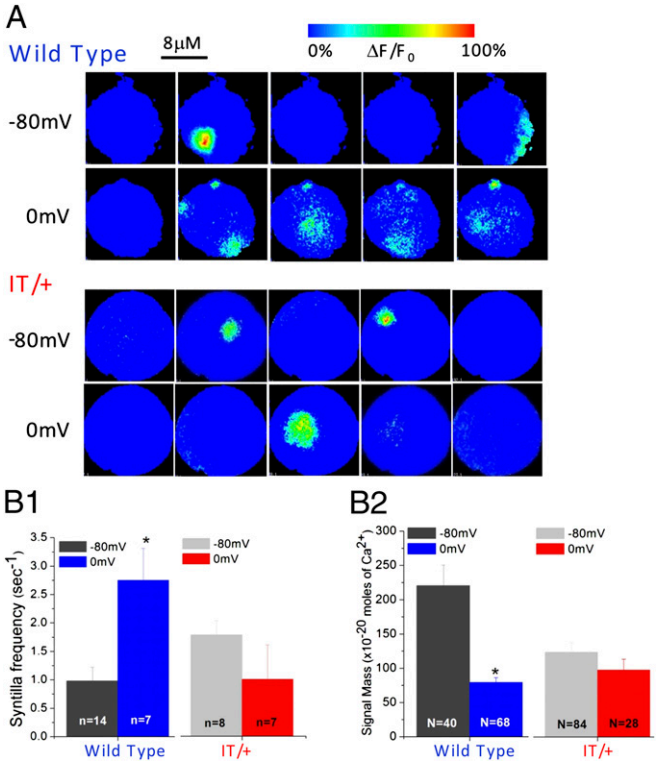

Fig. 2. VICaR is blocked in the IT/+ mutant. (*A*) Representative images of Ca^{2+} syntillas during 4-s recordings at −80 mV and 0 mV in the absence of extracellular Ca^{2+} and using fluo-3 as a Ca^{2+} indicator. In WT, depolarization to 0 mV increases the number of syntillas from two at −80 mV (first row) to six at 0mV (second row), but in IT/+ terminals the number of syntillas is not increased: two syntillas at −80 mV (third row) vs. one at 0 mV (fourth row). Syntilla frequency (*B1*) and Ca^{2+} signal mass (*B2*) in WT and IT/+ terminals at −80 mV and 0 mV. VICaR is apparent in the WT (*B1*, *Left*), where syntilla frequency is increased from 0.98 ± 0.24 s^{-1} ($n = 14$) at −80 mV to 2.75 ± 0.56 s^{-1} at 0 mV ($n = 7$), $P = 0.003$. VICaR is absent in IT/+ (*B1*, *Right*). Depolarization to 0 mV decreases the signal mass in WT (*B2*, *Left*), the signal mass was decreased from 220.6 ± 30.1 ×10^{-20} moles of Ca^{2+} ($N = 40$) at −80 mV to 79.3 ± 6.6 × 10^{-20} moles of Ca^{2+} ($N = 68$). In IT/+ (*B2*, *Right*), the signal mass was comparable at both voltage settings. *$P < 0.05$.

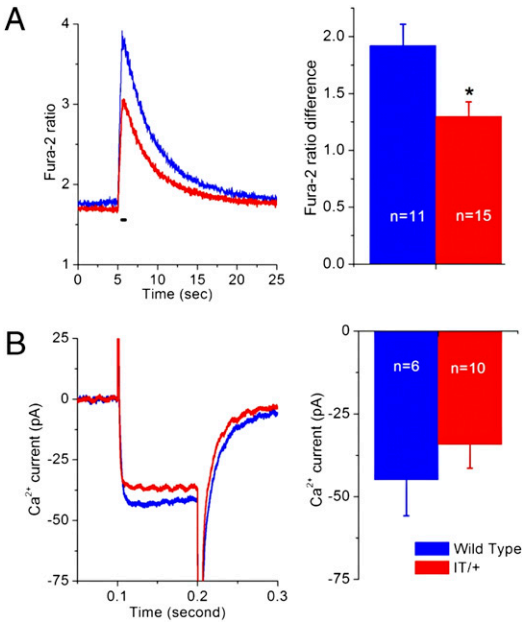

Fig. 3. Depolarization-induced changes in global cytosolic [Ca^{2+}] are smaller in IT/+ terminals than in WT. (*A*) Kinetics of changes in fura-2 ratio in WT (blue) and IT/+ (red) terminals upon depolarization from −80 mv to 0 mV for 500 ms. Traces (*Left*) are the mean values of the increase in fura-2 ratio for WT ($n = 11$) and IT/+ ($n = 15$). Bar graphs (*Right*) indicate a depolarization-induced significant increase in the fura-2 ratio in both WT and IT/+ terminals, but also reveal a significantly lower peak ratio in IT/+ compared with WT ($P = 0.009$). *$P < 0.05$. (*B*) Depolarization-induced whole cell Ca^{2+} currents were not significantly different.

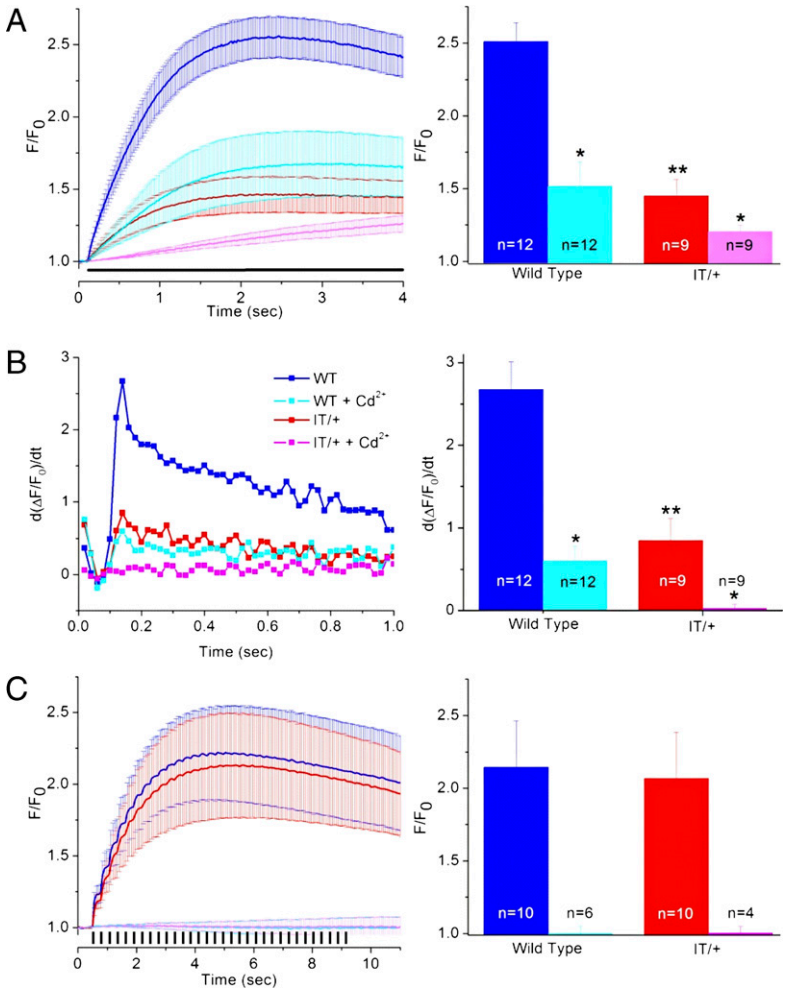

Fig. 4. VICaR is elicited by a prolonged plasmalemmal depolarizing not by a train of brief depolarizations. Nerve terminals were patch-clamped at physiological 2.2 mM extracellular [Ca^{2+}] with fluo-3 in the patch-pipette. F_0 is the average fluorescence in the first five images before the protocol and F is the fluorescence at each point in time over the whole nerve terminal. (*A*) Nerve terminals were depolarized continuously for 3.9 s to 0 mV in the absence or presence of 0.2 mM Cd^{2+}. (*Left*) F/F_0 increased in all samples upon depolarization (horizontal black bar). In IT/+ terminals the F/F_0 increase was significantly lower than in the WT, 1.46 ± 0.11 (n = 9) vs. 2.51 ± 0.13 (n = 12; P = 0.0001), respectively. (*Right*) The presence of Cd^{2+} reduced the increase in F/F_0 in WT to 1.52 ± 0.17 (n = 12), P = 0.00013) and to 1.21 ± 0.05 (n = 9), P = 0.05 in IT/+. The increase in fluorescence were measured over the last 2 s of recording. (*B*) First derivative of the fluo-3 fluorescence values recorded in *A*. (*Left*) Traces represent the average of derivatives in the first second of the recording. (*Right*) Bar graphs represent the average peak values at 0.14 s for the four conditions. The peak value was significantly different between WT and IT/+ (2.7 ± 0.3 vs. 0.8 ± 0.3, respectively, P = 0.0014). Addition of Cd^{2+} reduced the peak value in WT to 0.6 ± 0.2 (P = 0.00002), but in IT/+ terminals there was no detectable change in the peak value. (*C*) Nerve terminals were depolarized with short depolarizations (32 depolarizations of 80 ms, as indicated by vertical bars, separated by 280 ms), (*Left*) Similar F/F_0 increase in WT (blue) and IT/+ (red). (*Right*) Bar graphs show that NS80 induced an F/F_0 increase of 2.14 ± 0.32 in WT (n = 10) and 2.07 ± 0.32 in IT/+ (n = 10). In the presence of 0.2 mM Cd^{2+}, there were no increases in fluorescence in WT (n = 6) and IT/+ (n = 4). Measurements of the increase in fluorescence were made from the sixth second of the recording to the end of the stimulation (11.8 s). *P < 0.05; **P value Bonferroni adjusted.

Discussion

Two main conclusions follow from the work reported here on IT/+ mice. First, the I4895T CCD mutation, which we have found to give rise to myopathic changes in skeletal muscle, also has a neuronal phenotype, a unique demonstration of a neuronal phenotype for a *RyR1* mutation. Second, RyR1 mediates VICaR in hypothalamic magnocellular nerve terminals, as it does in skeletal muscle.

We had previously demonstrated that DHPRs and RyRs provide the molecular basis for VICaR in the nerve terminals (6). Here we implicate the type 1 RyR definitively by showing an effect of the *RyR1* IT/+ mutation on VICaR. In itself, this finding does not rule out an additional role for RyR2 as well, because both are abundant in these nerve terminals (6). It may be that VICaR works through DHPR activation of RyR1, and Ca^{2+} release from RyR1 activates RyR2 by CICR to yield amplification and a visible syntilla. The *RyR1* IT/+ mutation is proposed to be located in the pore region and that is the reason why it manifests decreased permeation. Lower conductance in the RyR1 IT/+ mutant might then result in insufficient Ca^{2+} release to trigger RyR2; hence, the frequency of visible syntillas drops. This process is analogous to the mechanism in amphibian skeletal muscle where the DHPR activates RyR1 directly and the resultant Ca^{2+} release, in turn, activates RyR3 via CICR (28).

The main conclusion is that the IT/+ mutant displays a neuronal phenotype. This finding is a unique functional and physiological demonstration that the type 1 RyR plays a role in nerve cells. It is of interest that chromaffin cells, which, like magnocellular neurons, are often used as a model system to study exocytosis, have no RyR1s and also no VICaR (29). Therefore, where RyR1 is found, VICaR might also be found. At the very least, it can no longer be assumed that CICR (30) is the only mechanism linking electrical activity in neurons to release from intracellular Ca^{2+} stores.

Our data are consistent with those in skeletal muscle where the mutation reduces RyR1 Ca^{2+} ion permeation in a manner that leads to a parallel reduction in both the magnitude (Fig. 4*A*) and rate (Fig. 4*B*) of RyR1-mediated Ca^{2+} release during EC coupling (15). Although the *RyR1* I4895T CCD mutation causes a core myopathy in our mouse line (14), we do not yet have evidence for a neuropathy in these same mice.

Spontaneous Ca^{2+} Release from Internal Stores in IT/+. Our results (Fig. 1) show that the syntilla frequency is higher in IT/+ than in WT at −80 mV in the presence of physiological [Ca^{2+}]. At first glance, this finding might seem to be at odds with the decrease in Ca^{2+} release on depolarization, although it clearly implicates type 1 RyR in resting release as well as VICaR. However, such a dual effect of the mutation is not necessarily contradictory. For example, the mutation, in addition to affecting conductance, may simply shift the voltage induction of Ca^{2+} release to negative potentials, causing less release on depolarization and more at rest. Or it may be that the DHPR exerts an inhibitory action on RyR1 at rest and depolarization removes the inhibition and causes activation. The *RyR1* mutation may weaken both interactions, resulting in more syntillas at rest and less Ca^{2+} release on depolarization. Additional work will need to be done to sort out such possibilities.

In cardiac myocytes, the occurrence of Ca^{2+} sparks at rest is used as an index of resting Ca^{2+} leak from the sarcoplasmic reticulum via RyR2 (31). However, as studied in bilayers and in cultured myotubes from IT/+ mutant mice, the IT mutation is not a leaky mutation: the presence of more than two IT mutant subunits in a tetramer has been shown to render RyR1 nonpermeant to Ca^{2+} (15). We found no increase in global [Ca^{2+}] at rest, so the increase in syntilla frequency is not sufficient to affect the detectable global [Ca^{2+}] (Fig. 3).

Role of RyR1 in Exocytosis. A special feature of hypothalamic magnocellular neurons is their direct involvement in the secretion of neuropeptides. We have shown that a syntilla does not elicit an exocytic event in the nerve terminals of these cells (32). The same finding is true in chromaffin cells, even though there is sufficient Ca^{2+} to do so if the Ca^{2+} of a syntilla were released at the site of the final exocytic step (29). These findings suggest that the Ca^{2+} from syntillas elicited by either type 1 RyRs (in nerve terminals) or type 2 (in chromaffin cells) is released into a microdomain different from the one where the final exocytic step occurs. Moreover, in chromaffin cells, we have found that syntillas that arise from RyR2s suppress exocytosis monitored amperometrically (33). A study on the porcine stress syndrome indicates that a similar mechanism may be present in the parvocellular neurons. In this case, boars that have a condition close to MH exhibit lower basal plasma ACTH (34). Because the *RyR1* R615C mutation that causes MH in these swine has a gain of function, the parvocellular neurons may have an increase in syntilla frequency that in turn would block the release of hormones. This ability of Ca^{2+} to have divergent or even antagonistic actions can be understood if the different targets of the Ca^{2+} released have low affinity and lie in different microdomains so that they are activated only by a nearby source of Ca^{2+}. In cell bodies of dorsal root ganglion neurons, however, focal Ca^{2+} transients arising from RyR3s do cause exocytosis, so that it is possible for such transients to have various effects, depending on cell type and localization within the cell (35).

Finally, the magnocellular neurons used in this study as a model are responsible for the level of the hormones oxytocin and vasopressin that have been associated with social behavior (36). Thus, it could be worthwhile to investigate whether RyR1-related myopathies might also be associated with variations in social behavior.

These findings also point out the importance of microdomains and brief focal Ca^{2+} transients. Among other things, the microdomains allow a single signal, Ca^{2+}, to have a wide array of effects (31). Focal Ca transients mediated by RyRs were first found as "sparks" in cardiac cells (37), where they are mediated by RyR2, and then under conditions of osmotic stress in skeletal muscle (38), where they are mediated by RyR1. In each of these cases, the sparks serve as elementary building blocks for global increases in Ca^{2+}, thus providing a clear physiological action. Next, sparks were found in smooth muscle (39) cells where a new dimension was added to their importance. In smooth muscle the sparks result in activation of nearby large Ca^{2+}-activated K^+ (BK) channels, giving rise to spontaneous transient outward currents that hyperpolarize the muscle and thus cause relaxation, the opposite effect of a rise in global cytosolic [Ca^{2+}] (39). The key to this duality is the relative insensitivity of BK channels to Ca^{2+} and their localization in the spark microdomain, where they are exposed to high concentrations of Ca^{2+} on the order of 10 μM, a level not reached by global [Ca^{2+}] (40–42). Thus, the microdomain in smooth muscle is the basis for Ca^{2+} to exert multiple, even opposite, effects and provides a precedent for their unexpected action in chromaffin cells (33).

Nerve terminals of the neurohypophysis secrete either oxytocin or vasopressin in response to bursts of action potentials (25). In situ, neurohypophysial terminals are closely packed, with tight interstitial spaces that limit diffusion, resulting in delayed external ion clearance. Stimulation of the intact neurohypophysis has been shown to increase external K^+ within the first 3 s (24). This increase in external K^+ induces a constant depolarization of the nerve terminals during the burst of action potentials. Thus, in the isolated terminals without the in situ restrictions on diffusion, long depolarization is necessary to mimic the physiological situation (43).

Our data show that long depolarization is more effective than a train of action potentials in activating VICaR. Hence, we propose a model in which each action potential lets Ca^{2+} enter via the N-type Ca^{2+} channels, causing secretion (44, 45) but, in addition, the long depolarization also activates VICaR via an interaction between L-type Ca^{2+} channels and RyR1. Thus, Ca^{2+} from extracellular spaces that activates exocytosis and Ca^{2+} released from intracellular stores via RyRs may enter different microdomains. For example, a burst of action potentials would trigger exocytosis, but the eventual buildup of K^+ and sustained depolarization would favor VICaR, syntilla generation, and perhaps suppression of exocytosis, which might act as a brake on exocytosis. It is evident from these considerations that the precise effect of VICaR and syntillas on exocytosis is potentially quite complex and needs to be carefully teased apart.

Materials and Methods

Animal Handling. Experimental protocols for animal research were approved by the Institutional Animal Care and Use Committees at both the University of Massachusetts Medical School and the University of Toronto. The generation and genotyping of IT/+ mice was described previously (16). For experiments, IT/+ mice, generated on a Sv129 background, were crossed with WT 129S2/SvPasCrl mice (Charles River).

Whole-Terminal Patching. For experiments, the mice of either sex and 10–12 wk of age were quickly killed by cervical dislocation, in accordance with local Institutional Animal Care and Use Committee guidelines (protocol A-124 to J.V.W. and A-1964 to V.D.C.). The hypothalamic magnocellular nerve terminals were freshly prepared as described previously (3). Tight-seal, "whole-terminal" recording on nerve terminals, was done with an EPC10 HEKA amplifier. Pipette solution was: 0.05 mM K_5fluo-3 or K5fura-2 (Molecular Probes), 135 mM KCl, 2 mM $MgCl_2$, 30 mM Hepes, 4 mM MgATP, 0.3 mM Na-GTP, pH 7.2. Bath solution was: 135 mM NaCl, 5 mM KCl, 10 mM Hepes, 10 mM Glucose, 1 mM $MgCl_2$, and 2.2 mM $CaCl_2$, pH 7.2. For the Ca^{2+}-free bath solution $CaCl_2$ is removed and 0.2 mM EGTA is added. To prevent depletion of Ca^{2+} from internal stores, the terminals remained in Normal Locke's solution (2.2 mM Ca^{2+}) until the beginning of the experiment, and the duration of the Ca^{2+}-free protocol was ~15 min (40).

To measure the magnitude of the plasmalemmal Ca^{2+} current in Fig. 3*B* in whole-cell configuration, the internal solution was changed to block

outward current and isolate the Ca^{2+} current: 130 mM NMG-Cl, 10 mM CsCl, 30 Hepes, 2 mM Mg-ATP, and 0.3 mM Tris-GTP. Moreover, TTX (1 μM) was added in the external solution to block Na^+ current. From a holding potential of −80 mV, we used 100-ms positive steps from −70 mV up to +50 mV in 10-mV increments and 60 s between each step. After a control protocol, we "puffed" Cd^{2+} for 2 min and then we constructed a new current voltage plot protocol while Cd^{2+} was still being puffed. No inward current could be recorded in the presence of Cd^{2+}. Only the value of the current at 0 mV was reported.

Reagents (from Sigma, unless otherwise noted) were bath perfused or delivered by a "picospritzer" (General Valve). Terminals were suspended from the tip of the pipette, out of contact with the floor of the chamber.

Fluorescence Recordings. We used the ratiometric indicator fura-2. The data reported represents the 340/380 nm excitation ratio for fura-2 that is representative of global cytosolic [Ca^{2+}] (46, 47). For Fluo-3, fluorescence images were obtained with a custom-built wide-field digital imaging system at 50 Hz (exposure 10 ms) (40). The terminals were imaged as described previously (3). Subsequent image processing and analysis was performed off line using a custom-designed software package. Two measures of Ca^{2+} were used: one to assess the properties of transient, focal increases in Ca^{2+} (i.e., Ca^{2+} syntillas) in a quantitative fashion, and another to assess global increases in Ca^{2+}.

Signal Mass. To assess the properties of Ca^{2+} syntillas and do so quantitatively, the signal-mass approach was used. Briefly, with this technique the total amount of Ca^{2+} released in a syntilla is measured with the Ca^{2+}-sensitive dye, fluo-3. The signal mass method is described in detail in ZhuGe et al. (27) and an adaptation to the magnocellular nerve terminals in De Crescenzo et al. (3), where the calibration to relate measured increase in fluorescence to the total amount of Ca^{2+} released in a single syntilla is also described.

Data Analysis. In all cases, data are reported as mean ± SEM; *N* is the number of syntillas that are used in the analysis of signal mass and *n* is the number of observations. Statistical analysis of differences was made with unpaired, two-tail *t* test, and the *P* values have been Bonferroni-adjusted (denoted by **), as appropriate, with $P < 0.05$ considered significant (denoted by *).

ACKNOWLEDGMENTS. We thank Drs. R. Dirksen (University of Rochester School of Medicine and Dentistry) and R. ZhuGe (University of Massachusetts Medical School) for interesting and helpful discussions. This study was supported by Grant HL21697 (to J.V.W.) from the National Institutes of Health; Grant 0835580D (to V.D.C.) from the American Heart Association; and Grant MOP-3399 (to D.H.M.) from the Canadian Institutes of Health Research.

1. Collin T, Marty A, Llano I (2005) Presynaptic calcium stores and synaptic transmission. *Curr Opin Neurobiol* 15:275–281.
2. Gleichmann M, Mattson MP (2011) Neuronal calcium homeostasis and dysregulation. *Antioxid Redox Signal* 14:1261–1273.
3. De Crescenzo V, et al. (2004) Ca2+ syntillas, miniature Ca2+ release events in terminals of hypothalamic neurons, are increased in frequency by depolarization in the absence of Ca2+ influx. *J Neurosci* 24:1226–1235.
4. Ouardouz M, et al. (2003) Depolarization-induced Ca2+ release in ischemic spinal cord white matter involves L-type Ca2+ channel activation of ryanodine receptors. *Neuron* 40:53–63.
5. Berrout J, Isokawa M (2009) Homeostatic and stimulus-induced coupling of the L-type Ca2+ channel to the ryanodine receptor in the hippocampal neuron in slices. *Cell Calcium* 46:30–38.
6. De Crescenzo V, et al. (2006) Dihydropyridine receptors and type 1 ryanodine receptors constitute the molecular machinery for voltage-induced Ca2+ release in nerve terminals. *J Neurosci* 26:7565–7574.
7. Giannini G, Conti A, Mammarella S, Scrobogna M, Sorrentino V (1995) The ryanodine receptor/calcium channel genes are widely and differentially expressed in murine brain and peripheral tissues. *J Cell Biol* 128:893–904.
8. Lanner JT, Georgiou DK, Joshi AD, Hamilton SL (2010) Ryanodine receptors: Structure, expression, molecular details, and function in calcium release. *Cold Spring Harb Perspect Biol* 2:a003996.
9. Maclennan DH, Zvaritch E (2011) Mechanistic models for muscle diseases and disorders originating in the sarcoplasmic reticulum. *Biochim Biophys Acta* 1813:948–964.
10. Lynch PJ, et al. (1999) A mutation in the transmembrane/luminal domain of the ryanodine receptor is associated with abnormal Ca2+ release channel function and severe central core disease. *Proc Natl Acad Sci USA* 96:4164–4169.
11. Hernandez-Lain A, et al. (2011) De novo RYR1 heterozygous mutation (I4898T) causing lethal core-rod myopathy in twins. *Eur J Med Genet* 54:29–33.
12. Robinson R, Carpenter D, Shaw MA, Halsall J, Hopkins P (2006) Mutations in RYR1 in malignant hyperthermia and central core disease. *Hum Mutat* 27:977–989.
13. Ramachandran S, Serohijos AW, Xu L, Meissner G, Dokholyan NV (2009) A structural model of the pore-forming region of the skeletal muscle ryanodine receptor (RyR1). *PLOS Comput Biol* 5:e1000367.
14. Zvaritch E, et al. (2009) Ca2+ dysregulation in Ryr1(I4895T/wt) mice causes congenital myopathy with progressive formation of minicores, cores, and nemaline rods. *Proc Natl Acad Sci USA* 106:21813–21818.
15. Loy RE, et al. (2011) Muscle weakness in Ryr1I4895T/WT knock-in mice as a result of reduced ryanodine receptor Ca2+ ion permeation and release from the sarcoplasmic reticulum. *J Gen Physiol* 137:43–57.
16. Zvaritch E, et al. (2007) An Ryr1I4895T mutation abolishes Ca2+ release channel function and delays development in homozygous offspring of a mutant mouse line. *Proc Natl Acad Sci USA* 104:18537–18542.
17. Shafiq SA, Gorycki MA, Asiedu SA, Milhorat AT (1969) Tenotomy. Effect on the fine structure of the soleus of the rat. *Arch Neurol* 20:625–633.
18. Boncompagni S, Loy RE, Dirksen RT, Franzini-Armstrong C (2010) The I4895T mutation in the type 1 ryanodine receptor induces fiber-type specific alterations in skeletal muscle that mimic premature aging. *Aging Cell* 9:958–970.
19. Sharma MC, Jain D, Sarkar C, Goebel HH (2009) Congenital myopathies—A comprehensive update of recent advancements. *Acta Neurol Scand* 119:281–292.
20. Engel WK (1961) Muscle target fibres, a newly recognized sign of denervation. *Nature* 191:389–390.
21. Schmitt HP, Volk B (1975) The relationship between target, targetoid, and targetoid/core fibers in severe neurogenic muscular atrophy. *J Neurol* 210:167–181.
22. Dubowitz V, Sewry CA (2007) *Muscle Biopsy: A Practical Approach* (Saunders Elsevier, London).
23. Dubowitz V, Roy S (1970) Central core disease of muscle: Clinical, histochemical and electron microscopic studies of an affected mother and child. *Brain* 93:133–146.
24. Leng G, Shibuki K, Way SA (1988) Effects of raised extracellular potassium on the excitability of, and hormone release from, the isolated rat neurohypophysis. *J Physiol* 399:591–605.
25. Cazalis M, Dayanithi G, Nordmann JJ (1985) The role of patterned burst and interburst interval on the excitation-coupling mechanism in the isolated rat neural lobe. *J Physiol* 369:45–60.
26. Eberhard M, Erne P (1989) Kinetics of calcium binding to fluo-3 determined by stopped-flow fluorescence. *Biochem Biophys Res Commun* 163:309–314.
27. ZhuGe R, et al. (2000) Dynamics of signaling between Ca(2+) sparks and Ca(2+)- activated K(+) channels studied with a novel image-based method for direct intracellular measurement of ryanodine receptor Ca(2+) current. *J Gen Physiol* 116: 845–864.
28. Pouvreau S, et al. (2007) Ca(2+) sparks operated by membrane depolarization require isoform 3 ryanodine receptor channels in skeletal muscle. *Proc Natl Acad Sci USA* 104: 5235–5240.
29. ZhuGe R, et al. (2006) Syntillas release Ca2+ at a site different from the microdomain where exocytosis occurs in mouse chromaffin cells. *Biophys J* 90:2027–2037.
30. Verkhratsky A (2005) Physiology and pathophysiology of the calcium store in the endoplasmic reticulum of neurons. *Physiol Rev* 85:201–279.
31. Cheng H, Lederer WJ (2008) Calcium sparks. *Physiol Rev* 88:1491–1545.
32. McNally JM, De Crescenzo V, Fogarty KE, Walsh JV, Lemos JR (2009) Individual calcium syntillas do not trigger spontaneous exocytosis from nerve terminals of the neurohypophysis. *J Neurosci* 29:14120–14126.
33. Lefkowitz JJ, et al. (2009) Suppression of Ca2+ syntillas increases spontaneous exocytosis in mouse adrenal chromaffin cells. *J Gen Physiol* 134:267–280.
34. Weaver SA, Dixon WT, Schaefer AL (2000) The effects of mutated skeletal ryanodine receptors on hypothalamic-pituitary-adrenal axis function in boars. *J Anim Sci* 78: 1319–1330.
35. Ouyang K, et al. (2005) Ca2+ sparks and secretion in dorsal root ganglion neurons. *Proc Natl Acad Sci USA* 102:12259–12264.
36. Meyer-Lindenberg A, Domes G, Kirsch P, Heinrichs M (2011) Oxytocin and vasopressin in the human brain: Social neuropeptides for translational medicine. *Nat Rev Neurosci* 12:524–538.
37. Cheng H, Lederer WJ, Cannell MB (1993) Calcium sparks: Elementary events underlying excitation-contraction coupling in heart muscle. *Science* 262:740–744.
38. Tsugorka A, Ríos E, Blatter LA (1995) Imaging elementary events of calcium release in skeletal muscle cells. *Science* 269:1723–1726.
39. Nelson MT, et al. (1995) Relaxation of arterial smooth muscle by calcium sparks. *Science* 270:633–637.
40. ZhuGe R, et al. (1999) The influence of sarcoplasmic reticulum Ca2+ concentration on Ca2+ sparks and spontaneous transient outward currents in single smooth muscle cells. *J Gen Physiol* 113:215–228.
41. Pérez GJ, Bonev AD, Nelson MT (2001) Micromolar Ca(2+) from sparks activates Ca(2+)-sensitive K(+) channels in rat cerebral artery smooth muscle. *Am J Physiol Cell Physiol* 281:C1769–C1775.
42. Zhuge R, Fogarty KE, Tuft RA, Walsh JV, Jr. (2002) Spontaneous transient outward currents arise from microdomains where BK channels are exposed to a mean Ca(2+) concentration on the order of 10 microM during a Ca(2+) spark. *J Gen Physiol* 120: 15–27.
43. Marrero HG, Lemos JR (2010) Ionic conditions modulate stimulus-induced capacitance changes in isolated neurohypophysial terminals of the rat. *J Physiol* 588:287–300.
44. Dunlap K, Luebke JI, Turner TJ (1995) Exocytotic Ca2+ channels in mammalian central neurons. *Trends Neurosci* 18:89–98.
45. Fisher TE, Bourque CW (1996) Calcium-channel subtypes in the somata and axon terminals of magnocellular neurosecretory cells. *Trends Neurosci* 19:440–444.
46. Grynkiewicz G, Poenie M, Tsien RY (1985) A new generation of Ca2+ indicators with greatly improved fluorescence properties. *J Biol Chem* 260:3440–3450.
47. Becker PL, Singer JJ, Walsh JV, Jr., Fay FS (1989) Regulation of calcium concentration in voltage-clamped smooth muscle cells. *Science* 244:211–214.